PAPER

Evidence for topological features in the electronic and phononic bands of ZGeSb (Z = Hf, Zr, Ti) class of compounds

IOP Publishing Journal of Physics: Condensed Matter
J. Phys.: Condens. Matter **34** (2022) 445502 (9pp) https://doi.org/10.1088/1361-648X/ac8c13

Evidence for topological features in the electronic and phononic bands of ZGeSb (Z = Hf, Zr, Ti) class of compounds

Rishi G[1], Anusree C V[1] and V Kanchana*

Department of Physics, Indian Institute of Technology Hyderabad, Kandi, 502285 Sangareddy, Telangana, India

E-mail: kanchana@iith.ac.in

Received 10 June 2022, revised 15 August 2022
Accepted for publication 23 August 2022
Published 5 September 2022

Abstract

Nontrivial topological properties in materials have been found in either the electronic or the phononic bands, but they have seldom been shown in both for a compound. With the aid of first-principle calculations, our paper attempts to find topological features in the electron and phonon band structures of ZGeSb (Z = Hf, Zr, Ti) class of compounds. The electron band structure exhibits two nodal rings in each of these compounds. Furthermore, drumhead surface states (DSS) have also been shown. The phonon band structure depicts one nodal ring in each of these compounds. DSS is also seen in the phonon surface states. Layering possibility has also been explored in HfGeSb, which admits a nodal ring each in its electronic and phononic band structure. Finally, these compounds (bulk and mono-layer) possess Dirac points robust to spin–orbit coupling effects, with at least one such Dirac point with its linear dispersion extending to the Fermi energy. Therefore, these compounds fall under the topological nodal line metals class, which is rarely seen in materials. These compounds' theoretical nontrivial topological nature in their electronic and phononic band structure provides a profound grasp of electronic and phononic nodal-line physics and is a good candidate for experimental verification. The existence of Dirac points close to the Fermi level could also motivate one to look for extreme magnetoresistance in these compounds. Moreover, given their largely metallic nature, these compounds become an excellent arena for novel device applications.

Keywords: electronic structure and nodal line features, fermi surface, topological phonons

(Some figures may appear in colour only in the online journal)

1. Introduction

In an era where quantum materials research has gained traction, classifying materials based on their topological characteristics has become exceedingly important. Topological materials in particular garnered attention since the discovery of topological insulators [1]. Topological insulators are materials that have insulating bulk states, but conducting surface states. This property, however, is not unique to topological insulators alone, as some ordinary insulators exhibit them as well (because the electrons in the surface experience a weaker potential and hence new states different from the bulk states are formed, and these states could give rise to a conducting

[1] These authors contributed equally.
* Author to whom any correspondence should be addressed.

nature on the surface). The property that makes these topological materials (not just insulators) unique is that these surface states are necessarily protected by time-reversal symmetry. Several such materials that exhibit nontrivial topological properties have been theorized and proven experimentally.

The study of these topological materials has additional benefits which help us understand the behaviour of some particles that have been predicted to exist by the standard model but have not been observed in nature. As an example, if one takes the example of a Dirac-like band crossing, it can be seen that the spectrum of these crossings is identical to that of a Weyl fermion [2], a zero mass half-spin particle that has not been observed yet (to the author's knowledge). Recently, it has been shown that even semimetals [3–5] and metals [6] can have topological aspects to their band structure. These materials are called topological semimetals (TSMs)/topological metals (TMs), respectively.

TSMs/TMs can, in turn, be classified into different types. Some of the well-known ones are Dirac semimetals (DSMs), Weyl semimetals (WSMs), nodal line semimetals (NLSMs), Dirac metals, Weyl metals, and nodal line metals (NLMs). In DSMs and metals, one can observe the occurrence of bulk band crossings due to doubly degenerate bands. These bulk crossings are protected by both time-reversal and inversion symmetries. TSMs/TMs could also host other crystal symmetries (like non-symmorphic symmetries). WSMs and metals are formed when either one of the symmetries (time-reversal or inversion) is broken [7]. In NLSMs and NLMs, the symmetry-protected band crossings form one dimensional surface [8–12] like rings, chains, Hopf links, starfruit-like structures [13, 14]. Their shape, however, depends on the crystal symmetry. Recently, even their two-dimensional analogs have been observed, and they are called topological nodal surfaces. Several such TSMs/TMs have been realized through experiments using transport and spectroscopy measurements. Examples include Na_3Bi [15], Cd_3As_2 [16], TaAs [17, 18], TaP [19], $MoTe_2$ [20], ZrSiS [21], $PbTaSe_2$ [22], and LaBi [23].

TSMs/TMs have found applications in quantum information, and spintronics [24–29]. These applications arise because the TSMs/TMs can exhibit exotic states (like the Weyl fermion-like states). They also exhibit phenomenon like high-temperature superconductivity [30–32], Hall effect [33, 34], and unconventional optical response [35, 36], etc.

One of the ways through which one can quantify topology in a material is through topological invariants. Topological invariants are numbers that depend on the system but do not change under smooth deformations of the Hamiltonian (or, in other words, Homeomorphisms). Examples of such quantities are the first Chern number [37], Z_2 topological invariant [38], Z_4 topological invariant [39], etc. This article mainly focuses on the Z_2 invariant.

The concepts used to describe topology in the electron band structure can also be extended to describe topology in the phonon band structure. Topological features such as Dirac points [40], Weyl points [41], and nodal lines [42] have been proposed to exist in phonons as well. In tandem with these similarities between the electron and phonon topologies, the Hall effect has also been reported to exist in some phonon systems [43, 44]. These phonons play a vital role in several material properties like thermal conductivity, superconductivity, specific heat. The phonons are fundamentally different from the electrons because the phonons are Bosons, whereas the electrons are Fermions. Studying these topological features can provide us with an understanding of Bosonic particles that have not even been observed in nature. Several nodal features seen in TSMs have also been observed in the phonon states. For example, nodal-line phonon states have been predicted to exist in graphene [45]. Other examples include, doubly degenerate phonon states in transition-metal monosilicides [46], triply degenerate phonon states in TiS, ZrSe and HfSe [45, 47].

A prominent and well studied TSM is ZrSiS. This compound hosts several nodal-line features in its electronic band structure [21, 48]. Several other topological features are also observed in its electronic band structure [49]. It also exhibits a large magnetoresistance [50]. This could be attributed to the fact that this compound has Dirac points at the Fermi energy [51]. Due to the existence of Dirac nodal line features in its electronic band structure, the compounds that belong to the same family as ZrSiS are studied extensively for nodal line possibilities, with the probability of realizing new fascinating quantum phases using the colossal pool of material systems available in this family. Motivated by the fact that ZGeSb (Z = Hf, Zr, Ti) belongs to the same family, our paper investigates the topological features present in these compounds ZGeSb (even though this compound is largely metallic). The presence of topological features in both the electronic and phononic band structure of semimetals and metals is very rarely seen. One such example is the Li_2BaSi class of semimetals [52]. Our paper shows the existence of nodal line features in both the electronic and phononic band structure using first-principle calculations. Our paper also shows the existence of Dirac points in the electronic band structure (some of which are very close to Fermi level).

Lastly, this paper looks at the monolayer HfGeSb system. This study is possible due to the low exfoliation energy of HfGeSb [53]. The existence of Dirac points in the electron band structure and nodal rings in the electron and phonon band structures is highlighted. The presence of Dirac points near the Fermi energy with the linear regime of the Dirac cone crossing the Fermi energy has been correlated to extreme magnetoresistance [51]. We also show the existence of such Dirac points (ones in the vicinity of the Fermi energy) in the monolayer system. Due to this possibility, this system may be an excellent candidate for extreme magnetoresistance studies. Furthermore, the fact that the compounds have a high density of states at the Fermi energy coupled with the fact that the compounds exhibit topological features in the electron and phonon band structures motivates one to look for superconductivity possibility in these compounds [54, 55]. Finally, the topological features also makes this compound a possible candidate for

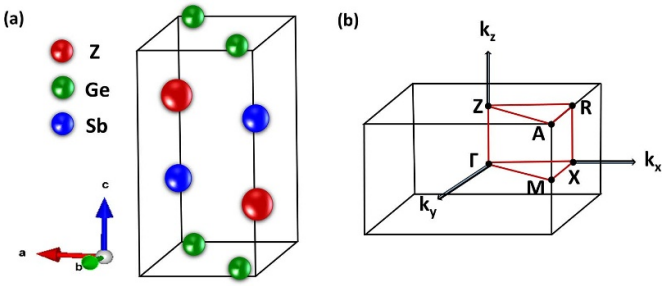

Figure 1. (a) Crystal structure of ZGeSb (Z = Hf, Zr and Ti). (b) Brilliouin zone with the high symmetry points showing the band path.

thermoelectric applications [56]. These facts also enhance the system's capability in device applications.

2. Computational details and crystal structure

The full geometry optimization for the studied compounds are performed using Vienna *Ab-initio* Simulation Package (VASP) [57–60] within generalized gradient approximation (GGA)-PBE [61] and local density approximation (LDA) [62] approximations and GGA-PBE results are found to be closer to the experimental parameters. The self-consistent calculations are performed in such a way that the energy and force are converged up to 10^{-6} eV and 10^{-2} eV Å^{-1} respectively. The Monkhorst–Pack scheme [63] is being used to generate the special k-mesh in the Irreducible Brillouin Zone and $10 \times 10 \times 5$ K-mesh has been chosen. The Brillouin zone integration has been done using the tetrahedron method [64]. The energy cut-off is set to 400 eV. The density functional perturbation method implemented in VASP with combination of Phonopy [65] has been opted for the phonon dispersion calculations. The electronic structure properties have been calculated for ground state energy eigenvalues. In order to analyze the topological nature, the tight-binding Hamiltonian is being generated in conjunction with the VASP code [66]. Further, the tight-binding parameters are fed to WannierTools [67] package, which employs an iterative Green's function [68] technique to compute the surface band structure using the Wannier functions and to obtain the surface state properties.

The investigated system ZGeSb crystallizes in ZrSiS-type structure with space group P4/nmm (129) [69]. Six atoms occupy three two-fold locations in each unit cell of ZGeSb's tetragonal structure: Z on 2c (1/4, 1/4, z1), Ge on 2a (3/4,1/4, 0) and Sb on 2c (1/4, 1/4, Z_2). The crystal structure along with bulk Brillouin zone with high symmetry points is depicted in figures 1(a) and (b). Two different exchange functional GGA and LDA are used for optimization and found that GGA results are consistent with the experimental parameters. The optimized parameters along with the experimental parameters are given in table 1. The investigated system possess inversion symmetry, time reversal symmetry and nonsymmorphic (glide plane and screw rotation) space group symmetry.

Table 1. Optimized parameters of ZGeSb along with experimental parameters.

	Experimental [69]		PBE [61]		LDA [62]	
Compound	a (Å)	c (Å)	a (Å)	c (Å)	a (Å)	c (Å)
HfGeSb	3.81	8.55	3.82	8.60	3.74	8.43
ZrGeSb	3.85	8.63	3.84	8.71	3.77	8.54
TiGeSb	3.70	8.21	3.72	8.25	3.64	8.07

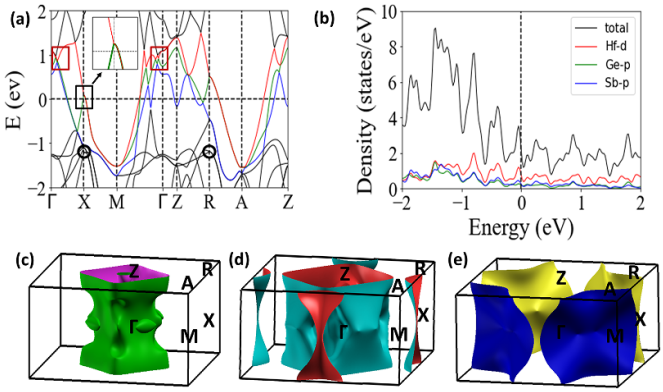

Figure 2. The band structure and density of states of HfGeSb in (a) and (b). The black box pin points to the Dirac point close to the Fermi energy, the red boxes pin point to the crossings that belong to the nodal ring and the black circles indicate the iso-energy Dirac points that form a Dirac nodal line along the *XR* path. The Fermi surface topology corresponds to blue, green and red bands in (c), (d) and (e).

3. Results and discussions

3.1. Electronic structure properties and topological nature

From the density of states plots given in figures 2(b), 3(b) and 4(b), these compounds are found to be largely metallic in nature. There are many crossing points near Fermi energy along path Γ – X – M – Γ as seen from figures 2(a), 3(a) and 4(a). The density of states along with partial orbital contribution are calculated to check the states contributing to these crossing points. The d-states of Z (Z = Hf, Zr and Ti) and p-states of Ge and Sb are dominating near Fermi level. Spin–orbit coupling's effect is found to be significant and the crossing points (except for the Dirac points at the TRIM points) are gapped out due to the lifting of the degeneracy.

In the systems ZGeSb (Z = Hf, Zr, Ti), there are three bands that contribute to the Fermi surface. The Fermi surfaces corresponding to the blue-coloured bands for the compounds ZGeSb are given in figure 2(c) (Z = Hf), figure 3(c) (Z = Zr) and figure 4(c) (Z = Ti). Along the $\Gamma - X - M - \Gamma$ path, there is only one crossing between Γ and *X*, and there is a triple crossing between M and Γ. The two additional crossings seen between *M* and Γ lead to the lemon-shaped Fermi surfaces (four of them due to symmetry) in the figure. Close to the *Z* point, there is a hemisphere-like Fermi surface in HfGeSb but is absent in ZrGeSb and TiGeSb. This can be inferred from the band structure. The valley-like Fermi surface whose minimum

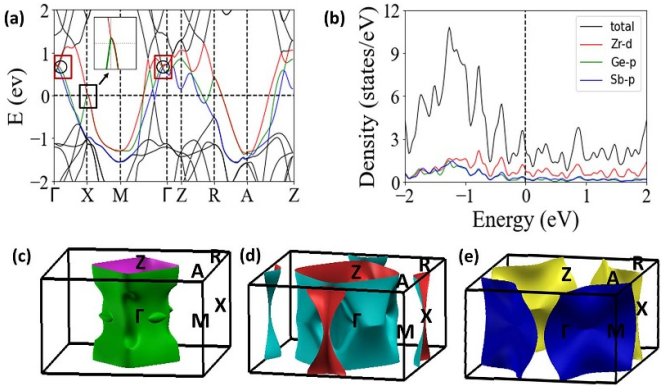

Figure 3. The bands structure and density of states of ZrGeSb in (a) and (b). The black box pin points to the Dirac point close to the Fermi energy, and the red boxes pin point to the crossings that belong to the nodal ring. The Fermi surface topology corresponding to blue, green and red bands in (c), (d) and (e).

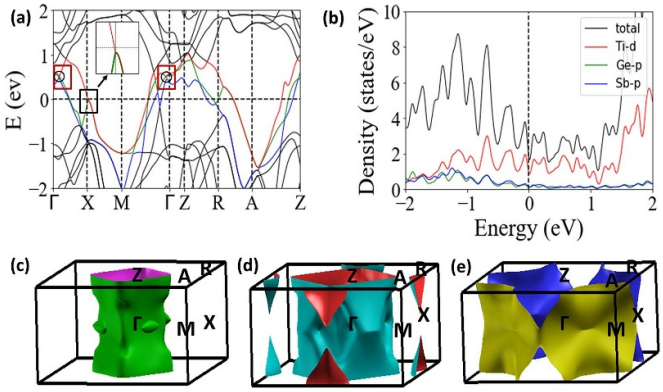

Figure 4. The band structure and density of states of TiGeSb in (a) and (b). The black box pinpoints the Dirac point close to the Fermi energy, and the red boxes pin point to the crossings that belong to the nodal ring. The Fermi surface topology corresponding to blue, green and red bands in (c), (d) and (e).

is at Z (in the band structure) does not cross the Fermi energy around Z in both ZrGeSb and TiGeSb, and only a single crossing is observed between Z and R. This leads to the absence of the hemispherical Fermi surface centred at Z that is seen in HfGeSb. The nature of this Fermi surface can be inferred from the band structure. Between Z and R (also between A and Z), the region between the points that cross the Fermi energy form a downward-facing parabola-like curve and is therefore a hole pocket. Apart from this Fermi surface, another distorted cylinder like surface can be seen in the Fermi surface of all three compounds.

The Fermi surfaces for the green coloured bands are shown in figure 2(d) (Z = Hf), figure 3(d) (Z = Ti) and figure 4(d) (Z = Zr). The band structure for all three compounds are very similar in profile and therefore all the features seen in the Fermi surfaces are also the same. Along the $Z-R-A-Z$ path, we see a double-crossing in the form of a valley between Z and R and a single crossing between A and Z. Here, the valley has its bottom-most point very close to the Fermi energy and therefore, the small quarter-spheres at the edges are seen only under higher resolution in the software. Since this is a valley, this Fermi surface forms an electron pocket. Apart from these small spheres there is also another larger Fermi surface resulting from the crossings in both the $\Gamma-X-M-\Gamma$ and $Z-R-A-Z$ paths.

The Fermi surfaces for the red coloured bands are shown in figure 2(e) (Z = Hf), figure 3(e) (Z = Zr) and figure 4(e) (Z = Ti). The Fermi surface profiles are nearly the same as a result of the similarity in the profiles of the band structure. In this case, no double Fermi energy crossings are seen between two adjacent TRIM (time-reversal invariant momentum) points. Therefore, no additional Fermi surfaces (apart from the flaps) are expected (and also observed) in the plots of these Fermi surfaces (at least not enclosing the high symmetry points). These four identical flaps are present as a result of mirror symmetry (this is also true for the other bands).

The appreciable SOC effect and the previous studies of the same family of materials motivate one to check the topological nature in this compound [21, 48, 49]. These compounds possess time-reversal and inversion symmetries. Any system that has inversion and time-reversal symmetries, Z_2 invariants (this is shown using analysis through parity of bands at high symmetry points) has non-trivial topology [70, 71]. The Z_2 invariant or the 'local Fermion parity' is one of the topological invariants that characterize the material's topological nature [1]. Furthermore, when the crystal possesses inversion symmetry, the value of Z_2 is equal to the product of the parity eigenvalues of all the occupied Bloch states at the TRIM points [72]. In three-dimensional systems, there are four such Z_2 invariants, namely ν_0, ν_1, ν_2, and ν_3. The quantity ν_0 is the value of the Z_2 calculated over all eight of the TRIM points, whereas the other three quantities (ν_1, ν_2, ν_3) are calculated over the TRIM points in three mutually orthogonal planes in the Brillouin zone. Each of these can take the values 0 or 1. If $\nu_0 = 1$, then the material is strong topological (with respect to Z_2). If $\nu_0 = 0$, but at least one of the other three is non-zero, the material is weak topological. Otherwise, the material is topologically trivial (with respect to Z_2) [73, 74].

To compute the Z_2 value, one uses the following formula:

$$(-1)^{\nu} = \prod_{TRIM} \delta_{TRIM} \tag{1}$$

where the product is over all the relevant TRIM points, and in the case of a crystal with inversion symmetry, we have,

$$\delta_p = \prod_m \xi_m(p) \tag{2}$$

$\xi(p)$ refers to the parity eigenvalue of the Bloch state at the TRIM point p, and the product m is over all the occupied states. The Z_2 values are given in table 2. These values are found using wannier tools. From the values given in the table, one can conclude that all three compounds are weak topological and are therefore topologically non-trivial.

Several Dirac points (fourfold degenerate points) are seen along the TRIM points X and R . From the SOC band structure plot figure 5(a), it is seen that these points are robust to SOC effects. The robustness is due to the fact that these compounds

Table 2. The parity calculated at high symmetry points and Z_2 invariants.

Compound	ν_0	ν_1	ν_2	ν_3
HfGeSb	0	1	0	0
ZrGeSb	0	0	1	0
TiGeSb	0	0	0	1

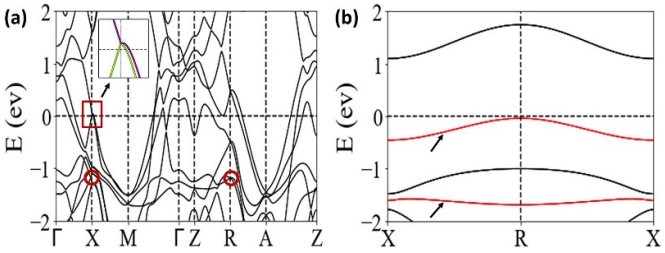

Figure 5. (a) HfGeSb band structure with the inclusion of SOC along with the Dirac points marked with a red box and red circles. (b) HfGeSb band structure (with SOC) along XRX path with the arrows pointing to the Dirac lines (four-fold degenerate) corresponding to the Dirac points marked in (a).

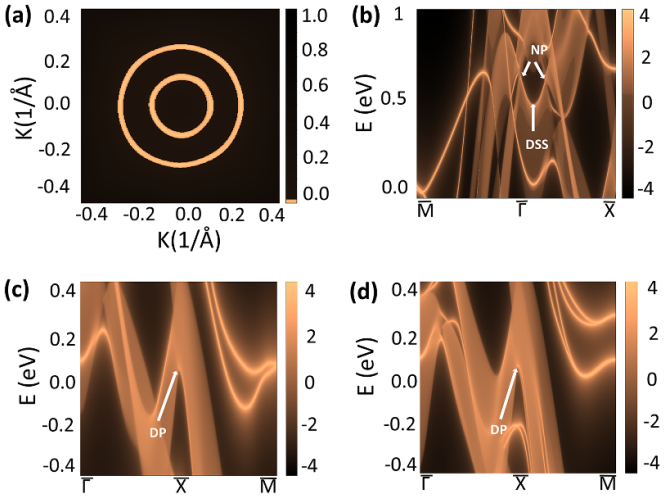

Figure 6. (a) Nodal rings present along (001) plane in HfGeSb compound. (b) Projected spectrum of the (0 0 1) surface with arrows pointing to the DSS arising from nodal points.

exhibit non-symmorphic symmetry (glide plane symmetry and screw rotational symmetry) [75]. The most notable of these Dirac points are the ones found very close to the Fermi energy (0.04 eV in HfGeSb, 0.03 eV in ZrGeSb, and −0.05 eV in TiGeSb) at the TRIM point with label X. The Dirac points are also shown in the surface state plot for HfGeSb in figures 6(c) and (d), where figure 6(c) corresponds to the case where SOC is not included, and figure 6(d) corresponds to the case where SOC is included. There are also Dirac points at the TRIM points X and R at an energy of about −1.6 eV, as highlighted with black circles in figure 2(a), for HfGeSb. A plot of the band structure along the path $X-R-X$ from figure 5(b) shows that these points are part of a Dirac nodal line (fourfold degenerate

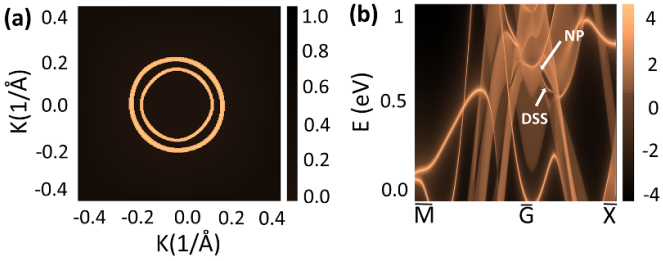

Figure 7. (a) Nodal rings present along (001) plane in ZrGeSb compound. (b) Projected spectrum of the (0 0 1) surface with arrows pointing to the nodal point, and the DSS.

bands). The other compounds under study also have a similar profile at their Dirac point, and hence those plots are not shown here. Using symmetry analysis, it was determined that the nodal line is protected by screw rotational symmetry. The screw rotation operator (C_{2y}) is given by:

$$C_{2y} : (x, y, z) \rightarrow \left(-x + \frac{1}{2}, y + \frac{1}{2}, -z\right). \tag{3}$$

Further analysis on this Dirac nodal line has not been performed since the nodal line is much below the Fermi energy, and hence not of much interest.

Aside from the differences in their contribution to the Fermi surface, the band structures profiles for the three compounds are very similar. The main focus of our paper will be the band structure in the $M-\Gamma-X$ region. Two sets of iso-energy band crossing points can be seen in all three band structures (the energies being 0.78 and 0.88 eV for HfGeSb, and 0.648 and 0.676 eV for ZrGeSb, and 0.44 and 0.47 eV for TiGeSb). These sets of iso-energy points contribute to the nodal rings observed in these compounds.

Motivated by the existence of the set of iso-energy points, the paper investigates the possibility of the existence of nodal rings. The Wannier tools program was used to check for these nodal line features. The surface state calculations in 001 plane are shown in figure 6(b) (for HfGeSb), figure 7(b) (for ZrGeSb), and figure 8(c) (for TiGeSb). In these plots, the white arrows point to the nodal points and the drumhead surface states (DSS), where the tail of the arrow specifies which one it corresponds to. Since these form iso-energy pairs, they are subjected to further tests to reveal the existence of nodal rings. Gap plane calculations are performed to confirm the existence of nodal rings. Figures 6(a), 7(a) and 8((a), (b)) display the continuous band crossings between the bands that display the iso-energy points in the band structure. The crossings form closed loops (or rings) in all three compounds. These rings are protected by mirror symmetry in the $z = 0$ plane. This computation confirms that these nodal points are indeed part of nodal rings. Therefore, ZGeSb compounds are topological NLMs. The plots figures 6(b), 7(b) and 8(c) also reveal the existence of DSS (marked with a white arrow). DSSs are surface states that emerge from nodal rings.

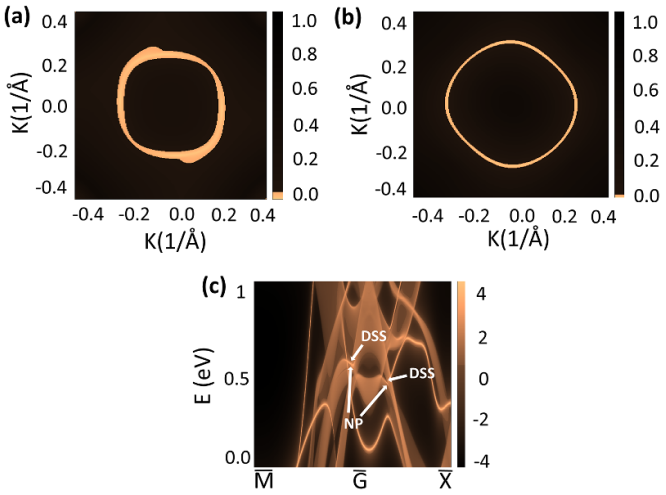

Figure 8. (a) and (b) Nodal rings present along (001) plane in TiGeSb compound. (c) Projected spectrum of the (0 0 1) surface with arrows pointing to the DSS arising from nodal points.

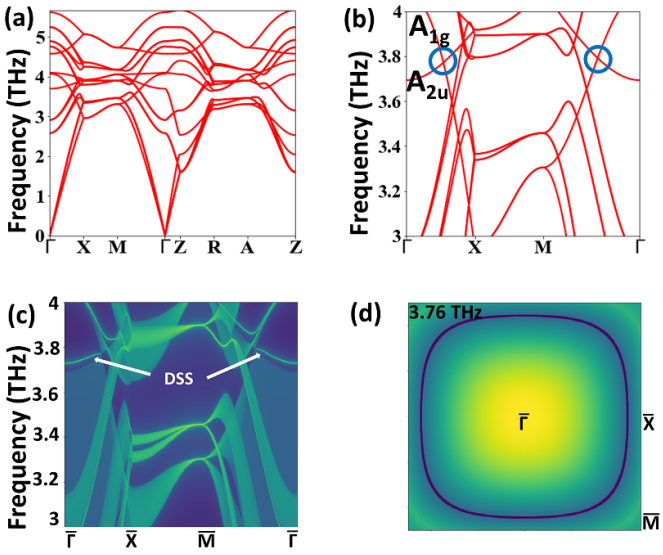

Figure 9. (a) Phonon band structure of HfGeSb. (b) Showing the nodal crossings between the corresponding symmetry states with opposite parity eigen values. (c) Phonon surface states plot of HfGeSb. (d) Constant frequency contour plotted at 3.76 THz.

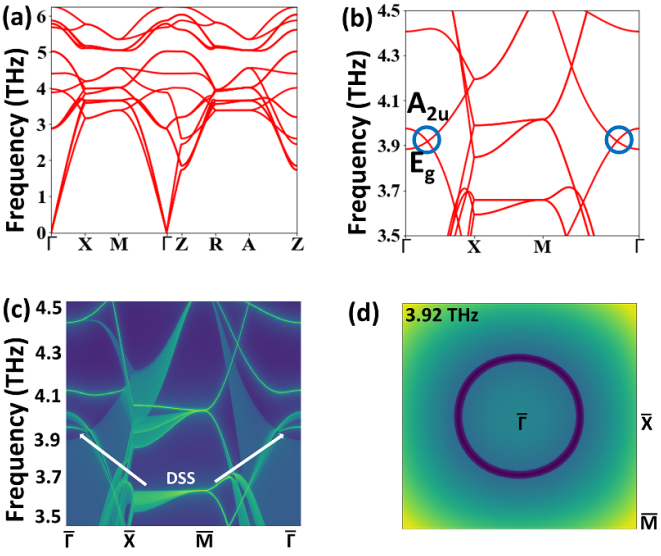

Figure 10. (a) Phonon band structure of ZrGeSb. (b) Showing the nodal crossings between the corresponding symmetry states with opposite parity eigen values. (c) Phonon surface states plot of ZrGeSb. (d) Constant frequency contour plotted at 3.92 THz.

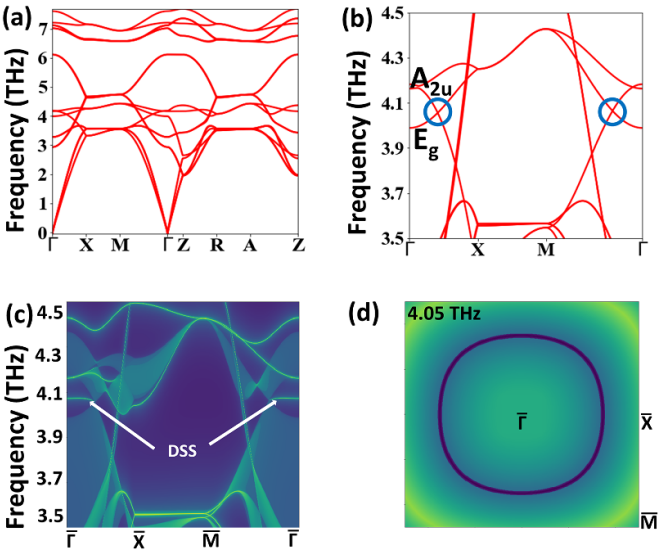

Figure 11. (a) Phonon band structure of TiGeSb. (b) Showing the nodal crossings between the corresponding symmetry states with opposite parity eigenvalues. (c) Phonon surface states plot of TiGeSb. (d) Constant frequency contour plotted at 4.05 THz.

3.2. Topological phonons in ZGeSb

The phonon band structure plots for the three compounds are shown in figures 9(a), 10(a) and 11(a). The absence of imaginary phonon frequencies assures the compounds' dynamical stability. The gap plane plots shown in figures 9(d), 10(d) and 11(d) confirm the existence of nodal rings formed by the pairs of iso energy points. In HfGeSb, the band crossing happens at a frequency of about 3.8 THz.

The crossing occurs between A_{2u} and A_{1g} symmetry states. This can be seen from the plots in figures 9(a) and (b). The opposite parity eigenvalues between the states ensure that the nodal crossings are protected against band hybridization.

In ZrGeSb, the band crossing takes place at a frequency of about 3.9 THz. Using symmetry analysis, it has been determined that the crossing occurs between E_g and A_{2u} states. Just like in HfGeSb, this results in the nodal crossings being protected against band hybridization. The results are shown in figure 10.

As shown in figure 11, the crossing in TiGeSb takes place between the same two symmetry states as in ZrGeSb, and hence it is protected. However, the crossing occurs at a frequency of about 4.05 THz. These compounds fall under the space group P4/nmm (129). From symmetry analysis it is found that the nodal ring is observed in the $k_z = 0$ plane and is

protected by glide mirror symmetry. The glide mirror operator ($\tilde{M}_z$) is defined by:

$$\tilde{M}_z : (x, y, z) \rightarrow \left(x + \frac{1}{2}, y + \frac{1}{2}, -z\right). \quad (4)$$

The phonon surface state calculations were then performed. These phonon surface state plots are shown in figures 9(c), 10(c) and 11(c), and are shown for the frequency range that encompasses the iso-energy crossing for the compounds. In each compound, one can observe DSS, similar to the electronic case. Such states have been marked with a white arrow. The DSS are fairly dispersionless in these compounds.

The topological nature of the phononic states is further confirmed by computing the Berry phase along a loop in the k-space that encompasses a point on the nodal ring (they have a Berry phase of π). The Berry phase (also called the geometric phase) describes the phase acquired by a state when it is subjected to an adiabatic evolution along a cycle in the parameter space (k-space in this case) [76]. This phase is the result of the geometric properties of the parameter phase. This quantity is computed using the following equation [77]:

$$\gamma_n[C] = i \oint_C A_n(k) dk. \quad (5)$$

Here, $A_n = i < n(k)|\nabla_k|n(k) >$ is called the Berry connection, where n refers to the nth eigen state (since the evolution is adiabatic, the nth eigen state remains the nth eigen state throughout the process), ∇_k is the gradient operation in the k-space, and C is the closed loop in the k-space.

3.3. HfGeSb monolayer studies

Among the three compounds, HfGeSb was chosen for monolayer studies. This compound was found to be cleavable with an exfoliation energy of 100.781 meV along the $a-b$ plane (see figure 12(a)). The following subsection deals with the electronic and phononic topological properties of monolayer HfGeSb.

3.3.1. Electron topology. The density of states plot from (figure 12(b)), shows that monolayer HfGeSb is metallic. From the band structure plot (figure 12(c)), one can observe several Dirac points (six at X and three at M), the most notable one being the Dirac points at X near Fermi energy (-0.026 eV), where the linear band dispersion crosses the Fermi energy for one of these points. Like bulk HfGeSb, the Dirac points in the mono-layer are also robust to SOC effects.

Due to the presence of Dirac points whose linear dispersion crosses the Fermi energy, this monolayer compound is an excellent place to look out for extreme magnetoresistance. The band structure plot also reveals the existence of iso-energy crossings at -0.1 eV. Motivated by this fact, gap-plane calculations were performed, and the result is shown in figure 12(d). From the gap-plane plot, it is evident that these iso-energy crossings indeed form a nodal ring. Finally, this system is found to be non-trivial with respect to Z_2 topology, which was shown with the help of Wannier Tools.

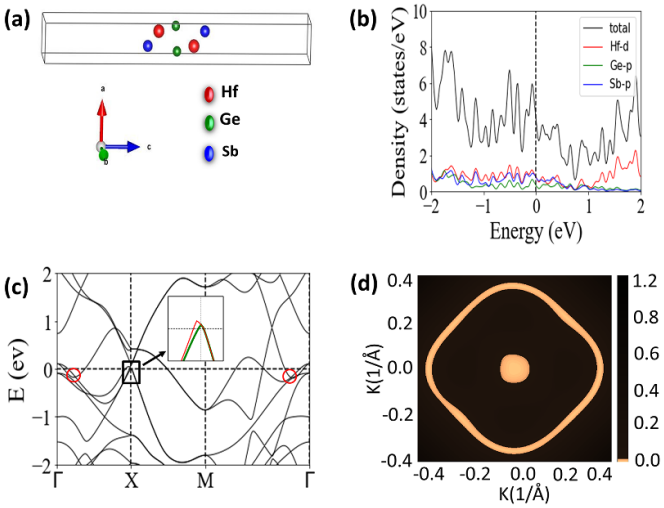

Figure 12. (a) Lattice structure of monolayer HfGeSb. (b) Density of States of HfGeSb monolayer. (c) The compound's band structure in the case where spin orbit coupling has not been included. The black box pin points to the Dirac points that are close to the Fermi Energy, and the red circles pin point to the points in the band structure that contribute to the nodal ring. (d) Gap-plane plot showing the nodal ring.

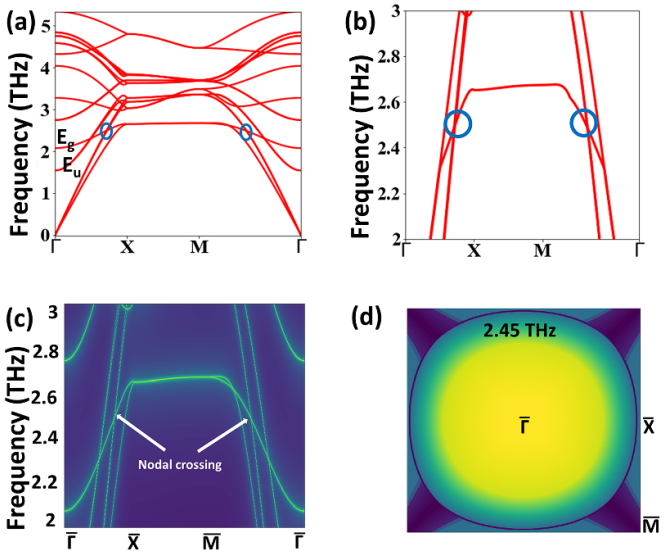

Figure 13. (a) Phonon band structure of monolayer HfGeSb. (b) Zoomed in plot of phonon band crossings. (c) Surface state plot of the phonons. (d) Gap plane calculation showing the nodal ring.

3.3.2. Phonon topology. The phonon band plot is shown in figure 13(a). Lack of imaginary phonon modes in the band plot assures the dynamical stability of the monolayer. One can also observe from the phonon band structure plot, the existence of several crossing points. Among these crossing points, the most notable ones are the iso-frequency crossing points close to 2.5 THz, which can be seen from the zoomed in phonon dispersion plot from figure 13(b). This prompts us to look for the possibility of nodal rings in the phonon band structure as well.

Computations similar to the ones performed for the bulk compounds prove the existence of a nodal ring at this frequency (see figures 13(c) and (d)). These crossing points also occur between E_u and E_g symmetry states, and the states have opposite parity eigenvalues, and therefore, protect the nodal crossings against band hybridizations. The topological protection is further confirmed by showing the nonzero value of Berry phase along a loop that contains a point that contributes to the ring (The Berry phase is found to be $-\pi$).

4. Conclusion

With the help of first-principle calculations, our paper shows the existence of topological nodal rings in the electron and phonon band structures of the ZGeSb (Z = Hf, Zr, Ti) class of compounds, and further confirmed these using Wannier tools calculations. Additionally, each of these compounds exhibit several Dirac points robust to SOC effects in their band structure, with one of them being in close proximity to the Fermi energy. Similar computations performed for monolayer HfGeSb, whose existence was confirmed through an exfoliation energy calculation, revealed a nodal ring in the electron and phonon band structure. The topological protection of the nodal rings in the phonon case (ZGeSb bulk and HfGeSb monolayer) was confirmed by proving the non-trivial Berry phase along a loop that contains a point that belongs to the ring. Additionally, the monolayer system also admitted several Dirac points robust to SOC effects in its band structure, with one of them having their linear band dispersion extending to the Fermi energy. Due to the existence of the Dirac points whose linear dispersion extends to the Fermi energy, ZGeSb (bulk and monolayer) can show extreme magnetoresistance. Furthermore, given the high density of states at the Fermi energy and the existence of electron and phonon topology, these compounds might host superconductive properties. The phonon topology also makes this compound an excellent candidate for thermoelectric applications. These breakthroughs (topological features) dramatically expand the number of topological electronic and phononic materials available, allowing for more in-depth studies of their structure-property relationships and opening new possibilities for future device applications.

Data availability statement

The data that support the findings of this study are available upon reasonable request from the authors.

Acknowledgments

The authors R G, A C V and V K would like to thank IIT Hyderabad and Centre for Development of Advanced Computing (CDAC) for computational facility. V K acknowledges DST project with Grant Number (CRG/2018/000220).

ORCID iD

V Kanchana https://orcid.org/0000-0003-1575-9936

References

[1] Hasan M Z and Kane C L 2010 *Rev. Mod. Phys.* **82** 3045–67
[2] Peskin M E and Schroeder D V 1995 *An Introduction to Quantum Field Theory* (Reading, MA: Addison-Wesley)
[3] Bansil A, Lin H and Das T 2016 *Rev. Mod. Phys.* **88** 021004
[4] Wang Z, Sun Y, Chen X Q, Franchini C, Xu G, Weng H, Dai X and Fang Z 2012 *Phys. Rev.* B **85** 195320
[5] Murakami S 2007 *New J. Phys.* **9** 356–356
[6] Wang Z *et al* 2016 *Phys. Rev. Lett.* **117** 056805
[7] Zyuzin A A, Wu S and Burkov A A 2012 *Phys. Rev.* B **85** 165110
[8] Yan Z, Bi R, Shen H, Lu L, Zhang S C and Wang Z 2017 *Phys. Rev.* B **96** 041103
[9] Bi R, Yan Z, Lu L and Wang Z 2017 *Phys. Rev.* B **96** 201305
[10] Si Li, Zhi M Y, Yugui Y and Shengyuan A Y 2020 *Front. Phys.* **15** 43201
[11] Bahari M and Hosseini M V 2019 *Phys. Rev.* B **99** 155128
[12] Bzdusek T, Wu Q, Ruegg A, Sigrist M and Soluyanov A A 2016 *Nature* **538** 75–78
[13] Chang G *et al* 2017 *Phys. Rev. Lett.* **119** 156401
[14] Singh B, Mardanya S, Su C, Lin H, Agarwal A and Bansil A 2018 *Phys. Rev.* B **98** 085122
[15] Wang Z, Sun Y, Chen X Q, Franchini C, Xu G, Weng H, Dai X and Fang Z 2012 *Phys. Rev.* B **85** 195320
[16] Wang Z, Weng H, Wu Q, Dai X and Fang Z 2013 *Phys. Rev.* B **88** 125427
[17] Lv B Q *et al* 2015 *Phys. Rev.* X **5** 031013
[18] Huang S M *et al* 2015 *Nat. Commun.* **6** 7373
[19] Chang G *et al* 2015 *Sci. Adv.* **1** e1501092
[20] Wang Z, Gresch D, Soluyanov A A, Xie W, Kushwaha S, Dai X, Troyer M, Cava R J and Bernevig B A 2016 *Phys. Rev. Lett.* **117** 056805
[21] Fu B B *et al* 2019 *Sci. Adv.* **5** 6459
[22] Bian G *et al* 2016 *Nat. Commun.* **7** 10556
[23] Jayita N *et al* 2017 *Nat. Commun.* **8** 13942
[24] Koshino M and Ando T 2010 *Phys. Rev.* B **81** 195431
[25] Zyuzin A A and Burkov A A 2012 *Phys. Rev.* B **86** 115133
[26] Hosur P and Qi X 2013 *C. R. Physique* **14** 857–70
[27] Fukushima K, Kharzeev D E and Warringa H J 2008 *Phys. Rev.* D **78** 074033
[28] Guin S N *et al* 2021 *Adv. Mater.* **33** 2006301
[29] Yang S A 2016 *SPIN* **06** 1640003
[30] Pang G M, Smidman M, Zhao L X, Wang Y F, Weng Z F, Che L Q, Chen Y, Lu X, Chen G F and Yuan H Q 2016 *Phys. Rev.* B **93** 060506
[31] Wang L S, Fang Y Q, Huang Y Y, Cheng E J, Ni J M, Pan B L, Xu Y, Huang F Q and Li S Y 2020 *Phys. Rev.* B **102** 024523
[32] Shimamura N *et al* 2018 *ACS Nano* **12** 10977–83
[33] Yang H Y *et al* 2020 *APL Mater.* **8** 011111
[34] Yang H Y *et al* 2021 *Phys. Rev.* B **103** 115143
[35] Liu Y, Yu Z M and Yang S A 2017 *Phys.Rev.*B **96** 121101
[36] Chang G *et al* 2017 *Phys. Rev. Lett.* **119** 206401
[37] Yasuhiro H 1993 *Phys. Rev. Lett.* **71** 3697–700
[38] Kane C L and Mele E J 2005 *Phys. Rev. Lett.* **95** 146802
[39] Araki H, Mizoguchi T and Yasuhiro H *Phys. Rev. Res.* **2** 012009
[40] Jin Y, Wang R and Xu H 2018 *Nano Lett.* **18** 7755–60
[41] Xiao M, Chen W, He W and Chan C 2015 *Nat. Phys.* **11** 920–24

[42] Stenull O, Kane C and Lubensky T 2016 *Phys. Rev. Lett.* **117** 068001
[43] Zhang L, Ren J, Wang J and Li B 2010 *Phys. Rev. Lett.* **105** 225901
[44] Liu Y, Xu Y, Zhang S and Duan W 2017 *Phys. Rev.* B **96** 064106
[45] Li J, Xie Q, Ullah S, Li R, Ma H, Li D, Li Y and Chen X Q 2018 *Phys. Rev.* B **97** 054305
[46] Zhang T, Song Z, Alexandradinata A, Weng H, Fang C, Lu L and Fang Z 2018 *Phys. Rev. Lett.* **120** 016401
[47] Xie Q, Li J, Ullah S, Li R, Wang L, Li D, Li Y, Yunoki S and Chen X Q 2019 *Phys. Rev.* B **99** 174306
[48] Neupane M *et al* 2016 *Phys. Rev.* B **93** 201104
[49] Mikitik G P and Sharlai Y V 2020 *Phys. Rev.* B **101** 205111
[50] Singha R, Pariari A K, Satpati B and Prabhat M *Proc. Natl Acad. Sci.* **114** 2468–73
[51] Okawa K, Kanou M, Namiki H and Sasagawa T 2018 *Phys. Rev. Mater.* **2** 124201
[52] Sharma V K, Singh B, Sarkar A B, Gupta M K, Mittal R, Agarwal A, Singh B and Kanchana V 2022 *J. Phys.: Condens. Matter* **34** 125502
[53] Jung J H, Park C-H and Ihm J 2018 *Nano Lett.* **18** 2759–65
[54] Jin K-H, Huang H, Mei J-W, Liu Z, Lim L-K and Liu F 2019 *npj Comput. Mater.* **5** 57
[55] Mazin I I and Antropov V P 2003 *Physica* C **385** 49–65
[56] Singh S, Wu Q, Yue C, Romero A H and Soluyanov A A 2018 *Phys. Rev. Mater.* **2** 114204
[57] Kresse G and Hafner J 1993 *Phys. Rev.* B **47** 558
[58] Kresse G and Furthmuller J 1996 *Comput. Mat. Sci.* **6** 15–50
[59] Kresse G and Furthmuller J 1996 *Phys. Rev.* B **54** 11169
[60] Kresse G and Joubert D 1999 *Phys. Rev.* **59** 1758
[61] Perdew J P, Burke K and Ernzerhof M 1996 *Phys. Rev. Lett.* **77** 3865
[62] Parr R G and Yang W 1994 *Density Functional Theory of Atoms and Molecules* (Oxford: Oxford University Press)
[63] Monkhorst H J and Pack J D 1976 *Phys. Rev.* B **13** 5188
[64] Blochl P, Jepsen O and Andersen O 1994 *Phys. Rev.* B **49** 16223
[65] Togo A, Oba F and Isao T 2008 *Phys. Rev.* B **78** 134106
[66] Marzari N, Mostofi A A, Yates J R, Souza I and Vanderbilt D 2012 *Rev. Mod. Phys.* **84** 1419
[67] QuanSheng W, ShengNan Z, Hai-Feng S, Matthias T and Alexey S 2018 *Compu. Phys. Commun.* **224** 405–16
[68] Sancho M L, Sancho J L and Rubio J 1985 *J. Phys. F: Met. Phys.* **15** 851
[69] Ozyar U F, Deligoz E and Colakoglu K 2015 *Solid State Sci.* **40** 92–100
[70] Wang Z, Xiao-Liang Q and Shou-Cheng Z 2012 *Phys. Rev.* B **85** 165126
[71] Fukui T and Hatsugai Y 2007 *J. Phys. Soc. Japan* **76** 053702
[72] Moore J E and Balents L 2007 *Phys. Rev.* B **75** 121306
[73] Jeffrey C Y, Teo L F and Kane C L 2008 *Phys. Rev.* B **78** 045426
[74] Liang F, Kane C L and Mele E J 2007 *Phys. Rev. Lett.* **98** 265004
[75] Schoop L M *et al* 2016 *Nat. Commun.* **7** 11696
[76] Berry M V 1984 *Proc. R. Soc.* A **392** 45–57
[77] Fang C, Chen Y, Kee H-Y and Fu L 2015 *Phys. Rev.* B **92** 081201